Optical-Sectioning Improvement in Two-Color Excitation Scanning Microscopy

CRISTINA IBÁÑEZ-LÓPEZ, ISABEL ESCOBAR, GENARO SAAVEDRA, AND MANUEL MARTÍNEZ-CORRAL*
Department of Optics, University of Valencia, E46100 Burjassot, Spain

KEY WORDS two-photon excitation; optical sectioning effect; beam shaping

ABSTRACT We present a new beam-shaping technique for two-color excitation fluorescence microscopy. We show that by simply inserting a properly designed shaded-ring filter in the illumination beam of smaller wavelength, it is possible to improve the effective optical sectioning capacity of such microscopes by 23%. Such an improvement is obtained at the expense of only a very small increasing of the overall energy in the point-spread-function sidelobes. The performance of this technique is illustrated by a numerical imaging simulation. *Microsc. Res. Tech. 64:96–102, 2004.* © 2004 Wiley-Liss, Inc.

INTRODUCTION

Optical sectioning is the key feature of optical microscopy when imaging three-dimensional (3D) samples. The use of wide-field optical fluorescence microscopes to image 3D biological or medical samples has the drawback that any image focused at a certain depth in the sample contains blurred information about the entire one. This fact gives rise to 3D images with strongly deteriorated contrast. This problem can be avoided by the use of single-photon fluorescence confocal scanning microscopes (SPCSM) (Pawley, 1995). The pinholed detection confers on these microscopes not only an important improvement in lateral resolution, but mainly an uncommon optical sectioning capacity. However, as pointed out by Cox and Sheppard (2004), in practical imaging the ideal concept of an infinitely small pinhole cannot be realized, particularly in fluorescence where light intensity is a limiting factor. Specifically, they found that when realistic pinhole sizes are used, the lateral resolution of SPCSM is essentially equivalent to that of wide-field fluorescence microscopes. Another serious problem of SPCSM is photobleaching, which appears since the entire sample is bleached when any single plane is imaged. Note that in single-photon fluorescence, bleaching depends on the time-averaged excitation intensity, which does not vary along the axial direction.

Other microscopes that efficiently perform optical sectioning are two-photon excitation (TPE) scanning microscopes. Such a nonlinear imaging technique was firstly reported in the early 1990s (Denk et al., 1990), and is based on the simultaneous absorption of two photons with nearly equal wavelengths, following which a single fluorescence photon is emitted (Göppert-Mayer, 1931). The excitation wavelength is typically twice as big as in the single-photon case. The fluorescence intensity is proportional to the square of the illumination intensity. Therefore, TPE microscopes have the ability of strongly limiting the excitation region. The overall fluorescence light is collected by a large-area detector, and the final image is synthesized from the 3D sampling of the object. TPE scanning microscopes inherently possess an optical sectioning capacity despite the absence of pinholed detection.

TPE scanning microscopes have the following advantages over SPCSMs: (1) Since there is no pinholed detection, there are no constraints on the practical attainment of the resolution predicted by the theory; (2) The absence of pinhole reduces the sensitivity to misalignment and increases the signal-to-noise ratio; (3) Photobleaching is restricted to the close neighborhood of the focusing plane. This is because photobleaching depends here on the time-averaged square of the intensity, which falls off strongly above and below the focal plane; and (4) The near-infrared light used for TPE is absorbed and scattered less by tissues, which allows deeper penetration of the excitation beam.

The resolving power of a microscope is usually evaluated in terms of its point spread function (PSF), which in the TPE case is defined as the fluorescence emission distribution generated by a light point. The fluorescence emission is proportional to the probability of simultaneous absorption of two low-energy photons. Since two statistically independent events have to occur, this probability is proportional to the square of the excitation intensity. The PSF of TPE microscopes is governed by diffraction laws and, therefore, is much wider in the axial direction than in the lateral direction. This implies that, in spite of their proverbial depth discrimination capacity, the axial resolution of TPE microscopes is much poorer than their lateral resolution. This fact leads to anysotropic 3D imaging quality.

Due to this reason, several attempts were made to improve the axial resolution of TPE microscopes. Let us cite the 4Pi-confocal microscope, in which two op-

*Correspondence to: Manuel Martínez-Corral, Departamento de Óptica, Universidad de Valencia, E46100 Burjassot, Spain. E-mail: manuel.martinez@uv.es

Received 27 February 2004; accepted in revised form 7 May 2004

Contract grant sponsor: Ministerio de Ciencia y Tecnología, Spain; Contract grant sponsor: Generalitat Valenciana, Spain; Contract grant number: DPI2003-4698; Spain; Contract grant number: grupos03/227.

DOI 10.1002/jemt.20073

Published online in Wiley InterScience (www.interscience.wiley.com).

© 2004 WILEY-LISS, INC.

posing, high-NA objectives are used to coherently illuminate the fluorescent probe and, therefore, to create a very narrow focal spot (Blanca et al., 2001). Unfortunately, the above method needs to strongly modify the microscope architecture and it is inherently limited to very thin samples. Other less efficient techniques, but mainly featured by their simplicity, are based on the insertion of a beam-shaping element in the illumination beam (Blanca and Hell, 2002; Martínez-Corral et al., 2003). However, although this technique can produce an important narrowness of the axial-PSF main peak, the effective improvement in axial resolution is reduced due to the increment of energy within the sidelobes, which inherently accompanies any axially-superresolving beam-shaping procedure.

This last drawback can be avoided if beam-shaping techniques are applied to an alternative type of TPE process, which uses two photons with different wavelengths. As stated by Denk et al. (1991), two-photon microscopes can also operate in sum of different frequency modes. This can be guaranteed by the presence of two illuminating beams with wavelengths λ_1 and λ_2 such that $\lambda_1^{-1} + \lambda_2^{-1} = \lambda_e^{-1}$,$\lambda_e$ being the single-photon excitation wavelength of the fluorescent sample. This nonlinear process, known as two-color excitation (TCE) fluorescence, has been extensively demonstrated in the past few years (Gryczynski et al., 1997; Lakowicz et al., 1996), and applied to different optical sectioning architectures (Lim and Saloma, 2002; Lindek and Stelzer, 1999; Xiao et al., 2003). The PSF of TCE microscopes is proportional to the product of two statistically-independent, differently-scaled excitation intensities, and is generated only in regions where the excitation beams overlap each other in space and time. This is the main advantage of TCE microscopes over TPE ones. The difference in scale between the two illumination PSFs permits the very efficient use of beam-shaping elements. Note that TCE microscopy combines the virtues of SPCSM, since the overall PSF is obtained as the product of two differently scaled PSFs, and of TPE, since the photobleaching is confined to a very small region. Then an axially superresolving beam-shaping element can be inserted in the beam of lower wavelength to produce a significant compression of the axial PSF, and a very small increase of the overall sidelobes' energy.

Superresolving beam-shaping elements have been successfully applied to improve the performance of many different imaging systems (Boyer, 2003; Chon and Gu, 2004; Pereira and van de Nes, 2004). The aim of the present research is to investigate the proper beam-shaping element for improving the optical sectioning of TCE microscopes. Specifically, we will show that it is possible to reduce the PSF main-peak width by 23% while preserving very high values (up to 96.5%) of spot fluorescence efficiency. This will lead to an effective, significant improvement of the optical sectioning capacity of the microscope. The utility of our method is illustrated by means of a numerical imaging experiment.

MATERIALS AND METHODS

Let us start by considering the PSF of a TCE fluorescence scanning microscope, schematically depicted in Figure 1. This function is given by

$$PSF(r,z;\lambda_1,\lambda_2) = |psf_1(r,z;\lambda_1)|^2 |psf_2(r,z;\lambda_2)|^2, \quad (1)$$

where, psf_i (i = 1,2) represent the amplitude PSFs of the illumination beams that, according to the scalar Debye formulation (Gu, 2000), can be expressed as

$$psf_i(r,z;\lambda_i) = \int_0^1 t_i(\rho) J_0\left(\frac{2\pi}{\lambda_i} r\rho sin\alpha\right) \exp\left\{-i2\pi z \frac{\sqrt{1-\rho^2\sin^2\alpha}}{\lambda_i}\right\} \frac{\sin^2\alpha}{\sqrt{1-\rho^2 sin^2\alpha}} \rho d\rho. \quad (2)$$

In this equation, α is the aperture angle of the objective lens, and $t(\rho)$ accounts for the amplitude transmittance of the objective-lens aperture stop. Besides, r and z are the cylindrical coordinates as measured from the focal point, whereas ρ is the normalized radial coordinate at the aperture stop. Equation 2 is, of course, a scalar approximation. As pointed out by Juškaitis (2003) this approximation works remarkably well up to angular apertures of about $\alpha = 60°$. More accurate calculations should be based on the vectorial Debye theory (Richards and Wolf, 1959).

The aim of this research is the achievement of significant improvement of axial resolution by application of the so-called PSF-engineering technique. Specifically, we propose to insert an axially-superresolving beam-shaping element in one of the excitation beams. Note that although, due to the depolarization phenomenon, the response of some beam-shaping elements should be treated in terms of the vectorial theory (Chon et al., 2002), the response of axially-superresolving elements can be accurately calculated in terms of the scalar theory (Martínez-Corral et al., 2004). It is clear from Eqs. (1) and (2), that the TCE PSF is obtained as the product of two independent PSFs, $|psf_1|^2$ and $|psf_2|^2$, which are scaled proportionally to λ_1 and λ_2, respectively. The beam-shaping element should be inserted in the illumination beam of smaller wavelength, which will be called beam-1 hereafter. There is one basic reason that arises against the use of superresolving elements in the illumination beam of bigger wavelength (beam-2). It results from the fact that, due to the wavelength mismatch, $|psf_2|^2$ is much wider than $|psf_1|^2$. Consequently, narrowing $|psf_2|^2$ would not produce any significant compression of the TCE PSF axial core but, conversely, it would reinforce the sidelobes' energy. However, when the filter is inserted in the beam-1, the axial compression of $|psf_1|^2$ is effectively transferred to the TCE PSF. Moreover, the high axial sidelobes of $|psf_1|^2$, are strongly reduced after the product with the minima of $|psf_2|^2$. It is then clear that the width of the TCE PSF core is limited by $|psf_1|^2$, whereas the sidelobes' overall intensity is constrained by $|psf_2|^2$. A scheme of the proposed TCE setup is shown in Figure 1.

To give an analytical foundation to the above heuristic analysis, it is convenient to focus our attention in the axial behavior of the TCE PSF, which is obtained after setting r = 0 in Eqs. (1) and (2). Specifically

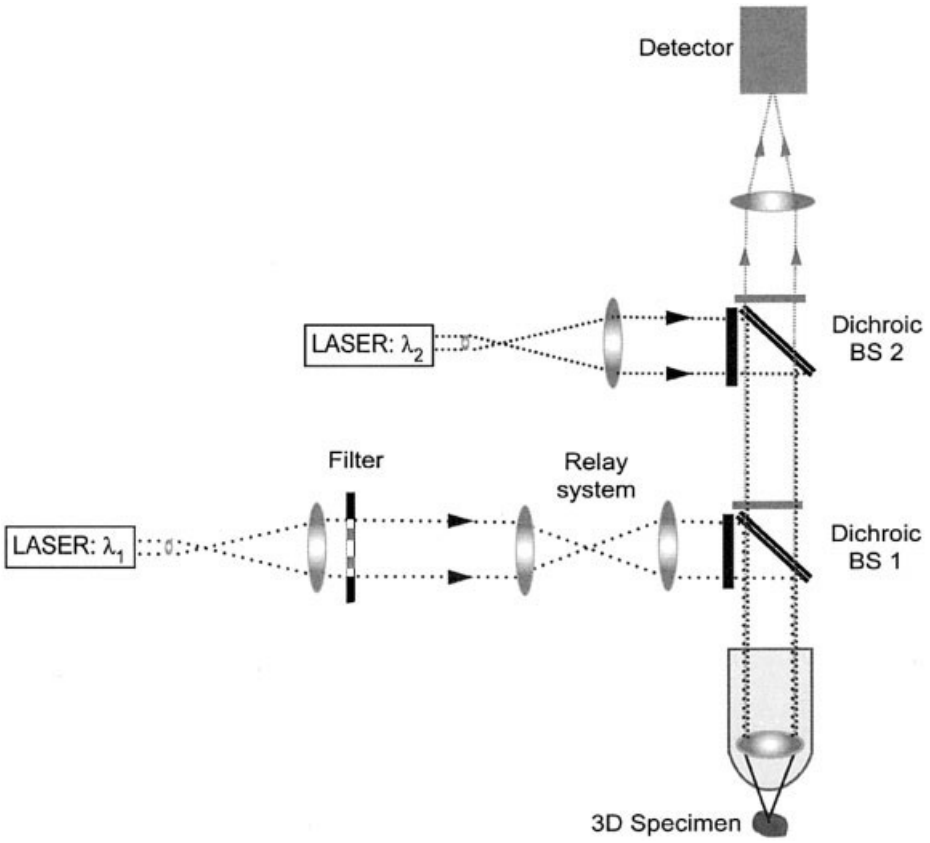

Fig. 1. Schematic geometry of the TCE scanning microscope. Relay lenses in beam-1 are used to image the beam-shaping element into the objective focal plane.

$$psf_i(r=0,z;\lambda_i)=\int_0^1 t_i(\rho)\exp\left\{-i2\pi z\,\frac{\sqrt{1-\rho^2\sin^2\alpha}}{\lambda_i}\right\}\frac{\sin^2\alpha}{\sqrt{1-\rho^2 sin^2\alpha}}\,\rho d\rho. \quad (3)$$

Under the nonlinear mapping

$$\zeta=\frac{\sqrt{1-\rho^2 sin^2\alpha}-\cos\alpha}{\cos\alpha-1}+0.5;\; q_i(\zeta)=t_i(\rho), \quad (4)$$

can be rewritten as

$$psf_i(z_N)=(1-\cos\alpha)\int_{-0.5}^{0.5} q_i(\zeta)\exp(-i2\pi\varepsilon_i z_N\zeta)d\zeta, \quad (5)$$

where the normalized axial coordinate is defined as

$$z_N=\frac{2z}{\lambda_0}sin^2(\alpha/2), \quad (6)$$

where $\varepsilon_i = \lambda_0 / \lambda_i$. Here λ_0 is the illumination wavelength for a TPE reference experiment with the same single-photon excitation wavelength, and therefore $\lambda_1 = \lambda_2 = \lambda_0$.

From Eqs. (1) and (5), it results that the axial PSF of the TCE fluorescence microscope is proportional to the product of the squared modulus of the 1D Fourier transforms of the mapped transmittances, $q_1(\zeta)$ and $q_2(\zeta)$, of the illuminating-beams aperture stops. Since no filter is inserted in the illuminating beam-2, $q_2(\zeta) = rect(\zeta)$ and, therefore, $|psf_2|^2$ equals to a sinc^2 function scaled proportionally to λ_2. To produce the effective improvement of the TCE axial resolution, it is necessary to insert in the illuminating beam-1 a filter with the ability to compress the main peak of its corresponding axial spot, but attenuating the reinforcement of sidelobe energy. This is the case of the family of filters known as the shaded-ring (SR) filters (Martínez-Corral et al., 2003). The SR filters simply consist of a purely absorbing ring with constant transmittance, which is centered on the objective lens aperture (see Fig. 2). Depending on the width and transmittance of the ring, different degree of main-peak compression can be achieved. Then a thorough study should be performed

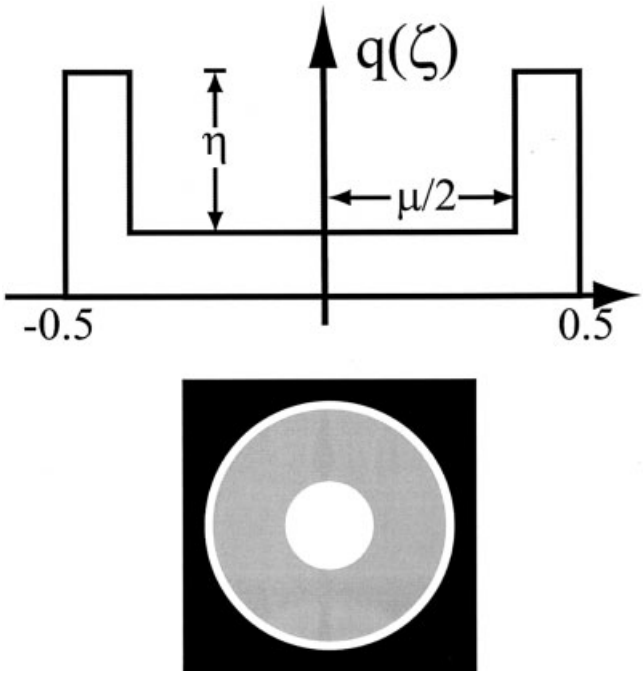

Fig. 2. Mapped transmittance of the SR filter and actual 2D representation.

to select the proper SR filter for our application. Our approach for this selection process is based on the concept of axial gain in resolution. A figure of merit is defined here as the quotient between the width of the main peak of the axial PSF of the TCE microscope in which the selected filter is inserted, and the corresponding to the reference TPE scanning microscope. Following an approach equivalent to that reported in (Martínez-Corral et al., 1999), and after straightforward calculations it is found that the axial gain is given by

$$G_{\mathrm{A}} = \sqrt{\frac{G_{SR}^2\varepsilon_1^2 + \varepsilon_2^2}{2}}, \tag{7a}$$

where, again, $\varepsilon i = \lambda_0 / \lambda_i$, and

$$G_{\mathrm{SR}} = \sqrt{\frac{1 - \eta\mu^3}{1 - \eta\mu}}. \tag{7b}$$

Construction parameters for the beam-shaping element η and μ are described in Figure 2. Note from the above equation that, in principle, the gain in axial resolution not only depends on the selected filter, but also on the relative values of the illumination wavelengths. Once selected the wavelengths, any pair (μ, η) fulfilling Eqs. (7) for a given G_A, correspond to SR filters with the same axial gain, but different sidelobes energy. Our goal in Results and Discussion is to select, given a wavelength relation $\kappa = \lambda_2 / \lambda_1$, the SR filter that produces the required gain in resolution and minimizes the sidelobes' overall energy.

RESULTS AND DISCUSSION

To start our procedure, we select a TCE fluorescence configuration suggested in other publications (Blanca and Saloma, 2001): $\lambda_0 = 700$ nm, $\lambda_1 = 656$ nm, and $\lambda_2 = 750$ nm (AMCA dye). In our numerical experiment, we will consider an objective of NA = 1.2 (water). To evaluate the ability of our technique for avoiding the sidelobes reinforcement, we introduce a second figure of merit, namely, the sidelobes-to-peak ratio (*SLPR*), defined as

$$SLPR = \frac{\int_{z_p}^{+\infty} PSF(r = 0,z;\lambda_1,\lambda_2)dz}{\int_{0}^{z_p} PSF(r = 0,z;\lambda_1,\lambda_2)dz}, \tag{8}$$

z_p being the coordinate of the first zero-intensity axial point.

To select the SR filter more adequate for our numerical experiment, in Figure 3a we have drawn several curves, each one with constant value for G_A but varying *SLPR*. As mentioned above, any point of the curve correspond to a different pair (η,μ). We select the gain $G_A = 1.25$, and within this curve the SR filter $\mu = 0.83$ and $\eta = 0.91$, which corresponds to the local minimum marked in Figure 3a. For this optimal filter, *SLPR* = 0.036, which is about 80% smaller than the *SLPR* ever obtained in TPE microscopy for similar values of the gain. Note that although in the right-hand extreme of the curve, the values for *SLPR* are lower than the selected one, those values correspond to filters with a very high value of μ, and therefore very small light throughput. In Figure 3b, we numerically evaluate axial PSF obtained with the filter inserted in beam-1. This PSF is compared with the one corresponding to the reference TPE experiment. Note that an important improvement (23% in terms of the FWHM) in axial resolution is obtained, and only a very small reinforcement of sidelobe energy. This effect is graphically illustrated in Figure 4 where we have represented the 3D PSFs described above. Note that the improvement in axial resolution is accompanied by only a small worsening in lateral resolution (1.7% in terms of the FWHM). In summary, the use of SR filters in TCE fluorescence microscopy produces an important improvement in the axial resolution at the expense of only a small worsening of light-spot efficiency (calculated as 100/(1+*SLPR*), which decreases from 99% in the reference TPE setup to 96.5% in the proposed TCE experiment.

When dealing with the imaging of 3D objects, the optical sectioning capacity of the system must be evaluated not only in terms of the 3D PSF, which is strictly valid only in case of point-like objects, but also in terms of the so-called integrated intensity, or equivalently its 1D Fourier transform, i.e., the axial component of the 3D OTF. Note that the axial OTF, which is a delta

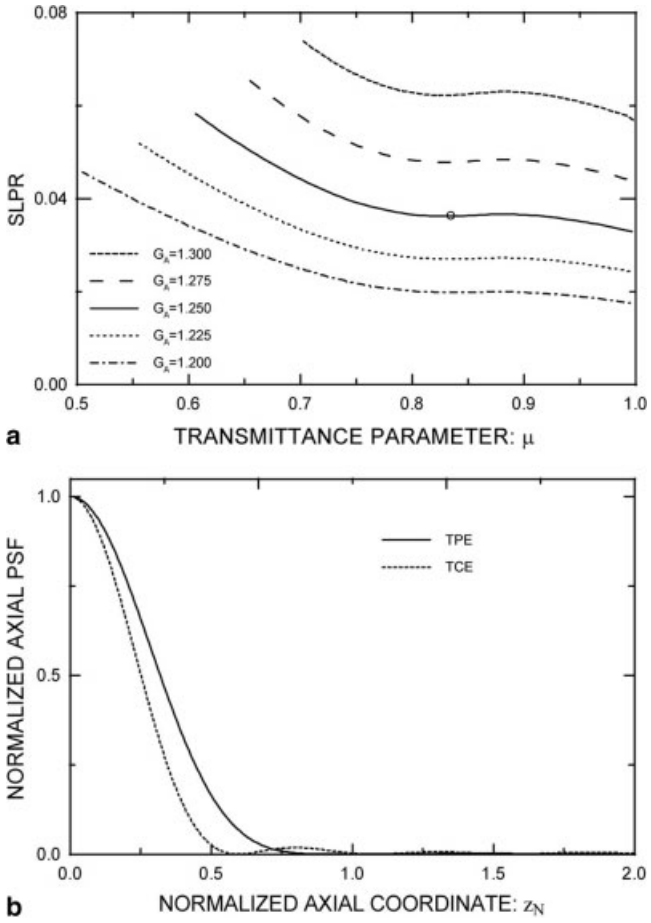

Fig. 3. **a:** *SLPR* values for families of filters with the same axial gain G_A. **b:** Comparison of axial PSFs corresponding to the proposed TCE setup and the reference TPE experiment.

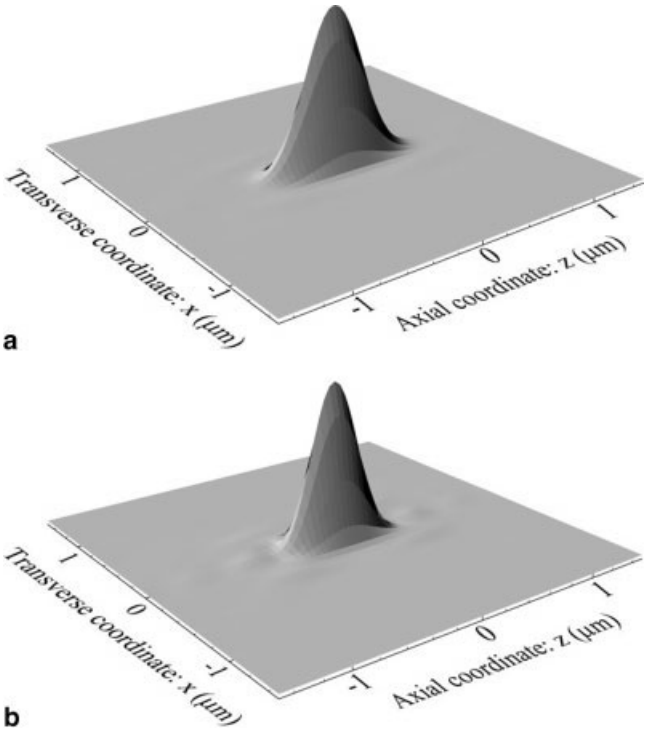

Fig. 4. 3D PSFs corresponding to (**a**) the TPE reference experiment; (**b**) the proposed TCE setup.

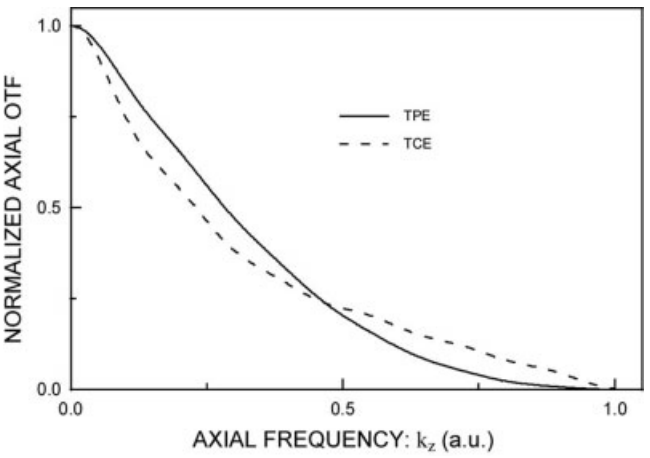

Fig. 5. Axial OTF for the same setups as in Figure 4.

function in conventional imaging systems, evaluates how efficiently the different axial frequencies of the 3D object are imaged. In Figure 5, we compare the axial OTF of our proposed TCE experiment with the one of the reference TPE setup. In the range of low axial frequencies, the performance of our method is, in relative terms, slightly worse than the reference TPE setup. However, in the range of medium and large axial frequencies (which define the finest details of the objects), the OTF provided by our system is between two and three times higher than the TPE one.

To illustrate the utility of our proposal, we have performed a numerical imaging experiment in which we calculate the resulting 3D image of a test object. We designed an elaborated 3D synthetic object consisting of two concentric spherical fluorescence labeled shells, as shown in Figure 6a. The dark band in the object allows to clearly visualize the improvement in resolution along the different directions passing through the focus. After convolution with the TCE PSF and with the TPE reference PSF, we obtained the simulated images shown in Figure 6b,c. Note from Figure 6 that in the axial direction the amount of blur in the image of the dark band (devoid of fluorescence) is significantly lower in the optimized TCE architecture proposed here.

An interesting question at this point is to find out the dependence of the performance of our method on the choice of λ_1 and λ_2 for a given excitation energy, or equivalently for a given λ_0. To perform this study, we have calculated, for varying values of the wavelengths ratio parameter, $\kappa = \lambda_2 / \lambda_1$, the optimum filter with $G_A = 1.25$. The pair (η, μ) is different for any value of κ. Note that the higher the value of κ, the wider $|psf_2|^2$ with respect to $|psf_1|^2$. This fact implies that for high values of κ, the transference of narrowness from $|psf_1|^2$ to the TCE PSF is more effective but, conversely, the reduction of sidelobes is less significant. As we show in

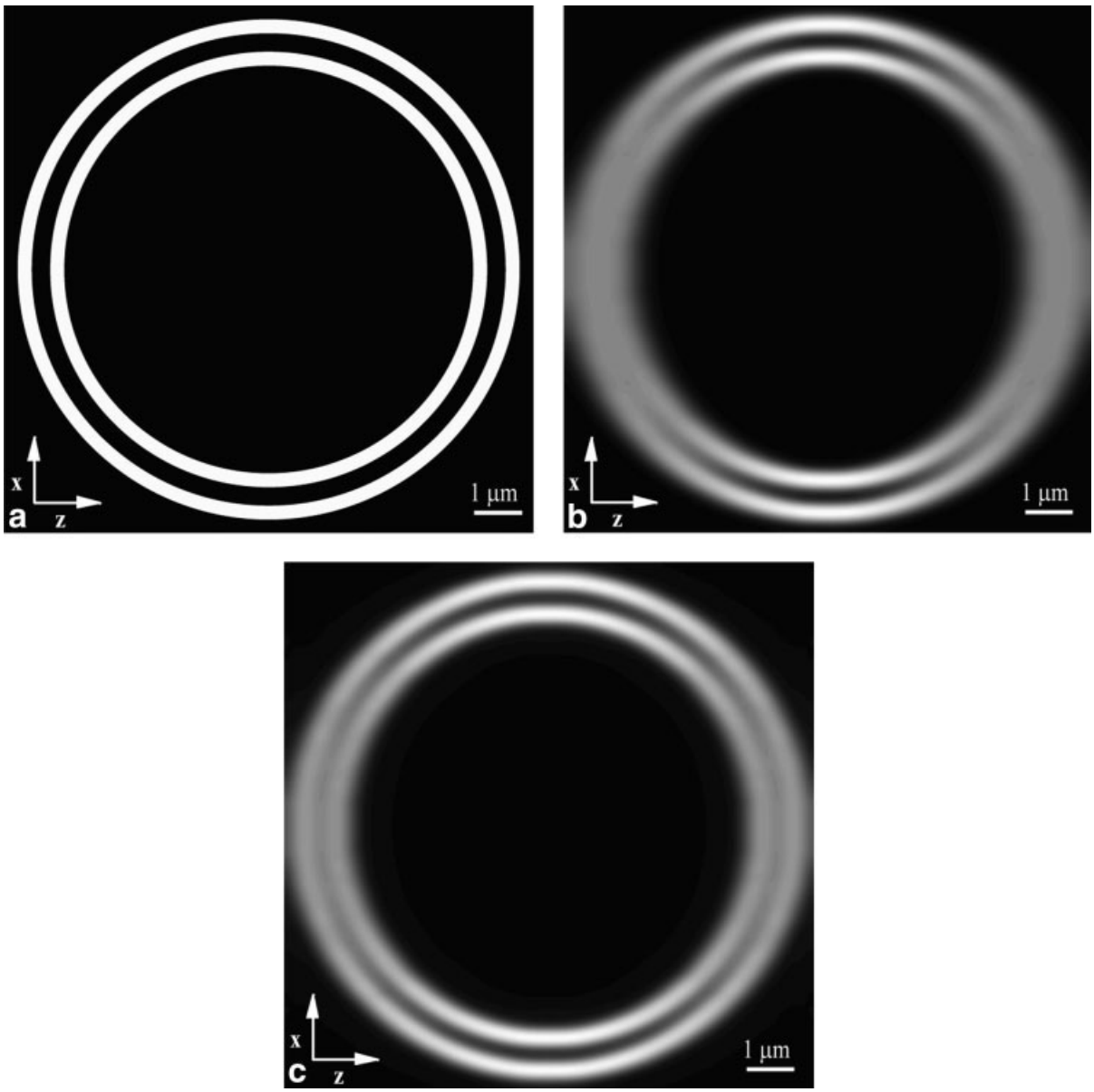

Fig. 6. Meridian section of: (**a**) Test object consisting of two concentric labeled shells; (**b**) calculated image for the TPE reference setup; (**c**) same but for the case of the proposed TCE architecture.

Figure 7, the overall performance of our method is quite insensitive to a variation of the wavelengths ratio κ. Specifically, the curve in Figure 7 corresponds to TCE architectures with the same axial gain G_A = 1.25 and κ varying from 1 to 2. Note that whereas the optimum $SLPR$ = 0.036, the value of this parameter is always under 0.060.

CONCLUSIONS

We have reported a method for achieving high optical sectioning in 3D fluorescence microscopy. The method combines the virtues of beam-shaping procedures with those of an alternative type of TPE process, which uses two photons with different wavelengths. We have shown that by this method it is possible to reduce the PSF main-peak width by 23% while preserving very high values (up to 96.5%) of spot fluorescence efficiency. This leads to a significant improvement of the optical sectioning capacity of the microscope. We have illustrated the power of our proposal by performing a numerical imaging experiment.

ACKNOWLEDGMENTS

This work has been funded by the Plan Nacional I+D+I (grant DPI2003-4698), Ministerio de Ciencia y Tecnología, Spain. C. Ibáñez-López gratefully acknowledges a pre-doctoral grant from the same institution. I. Escobar acknowledges a pre-doctoral grant from the

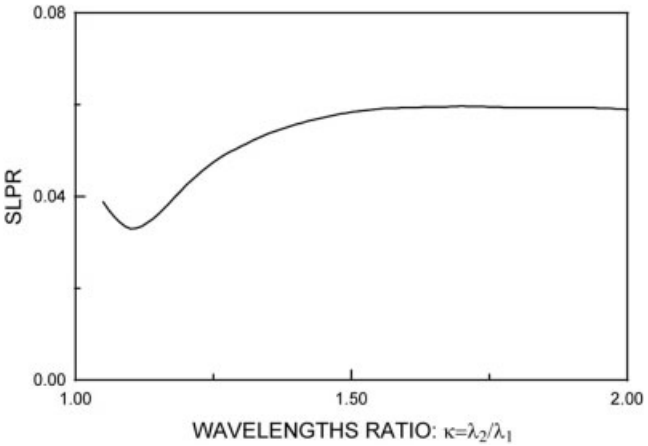

Fig. 7. *SLPRs* corresponding to TCE architectures with the same axial gain $G_A = 1.25$ but varying value for the wavelength ratio κ. This curve is a proof of the robustness of the proposed method that, although optimum for $\kappa = 1.10$, produces very small values of *SLPR* for a wide range of κ.

Ministerio de Educación y Ciencia, Spain. We also acknowledge the financial support from the Generalitat Valenciana, Spain (grant grupos03/227).

REFERENCES

Blanca CM, Hell SW. 2002. Axial superresolution with ultrahigh aperture lenses. Opt Express 10:893–898.

Blanca CM, Saloma C. 2001. Two-color excitation fluorescence microscopy through highly scattering media. Appl Opt 40:2722–2729.

Blanca CM, Bewersdorf J, Hell SW. 2001. Single sharp spot in fluorescence microscopy of two opposing lenses. Appl Phys Lett 79: 2321–2323.

Boyer G. 2003. 3D Behaviour of Frieden filters in confocal imaging. Micron 37:275–282.

Chon JW, Gu M. 2004. Scanning total internal reflection fluorescence microscopy under one-photon and two-photon excitation: image formation. Appl Opt 43:1063–1071.

Chon JW, Gan X, Gu M. 2002. Splitting of the focal spot of a high numerical-aperture objective in free space. Appl Phys Lett 81: 1576–1578.

Cox G, Sheppard CJR. 2004. Practical limits of resolution in confocal and non-linear microscopy. Microsc Res Tech 63:18–22.

Denk W, Strickler JH, Webb WW. 1990. Two-photon laser scanning fluorescence microscopy. Science 248:73–76.

Denk W, Strickler JH, Webb WW. 1991. Two-photon laser microscopy. US patent, 5,034,613, July 23.

Göppert-Mayer M. 1931. Über Elementarakte mit zwie Quantensprüngen. Ann Phys (Leipzig) 9:273–294.

Gryczynski I, Malak H, Lakowitz R. 1997. Two-color two-photon excitation of indole. Biospect 3:97–101.

Gu M. 2000. Advanced optical imaging theory. Berlin: Springen-Verlag.

Juškaitis R. 2003. Characterizing high numerical aperture microscope objective lenses. In: Török P, Kao FG, editors. Optical imaging and microscopy. Berlin: Springer.

Lakowicz JR, Gryczynski I, Malak H, Gryczynski Z. 1996. Two-color two-photon excitation fluorescence. Photochem Photobiol 64:632.

Lim M, Saloma C. 2002. Confocality condition in two-color excitation microscopy with two focused excitation beams. Opt Commun 207: 121–130.

Lindek S, Stelzer EHK. 1999. Resolution improvement by nonconfocal theta microscopy. Opt Lett 24:1505–1507.

Martínez-Corral M, Andrés P, Zapata-Rodríguez CJ, Kowalczyk M. 1999. Three-dimensional superresolution by annular binary filters. Opt Commun 165:267–278.

Martínez-Corral M, Ibáñez-López C, Saavedra G, Caballero MT. 2003. Axial gain in resolution in optical sectioning fluorescence microscopy by shaded-ring filters. Opt Express 11:1740–1745.

Martínez-Corral M, Martínez-Cuenca R, Escobar I, Saavedra G. 2004. Reduction of focus size in tightly focused linearly polarized beams. Appl Phys Lett (in press).

Pawley JB. 1995. Handbook of biological confocal microscopy. New York: Plenum Press.

Pereira SF, van de Nes AF. 2004. Superresolution by means of polarisation phase and amplitude pupil masks. Opt Commun 234:119–124.

Richards B, Wolf E. 1959. Electromagnetic diffraction in optical systems. II. Structure of the image field in an aplanatic system. Proc R Soc (Lond) A 253:358–379.

Xiao F, Wang G, Xu Z. 2003. Superresolution in two-color excitation fluorescence microscopy. Opt Commun 228:225–230.